ACS Sustainable Chemistry & Engineering

Research Article

Cite This: ACS Sustainable Chem. Eng. 2019, 7, 11194−11204

pubs.acs.org/journal/ascecg

Hierarchical Bulk Nanoporous Aluminum for On-Site Generation of Hydrogen by Hydrolysis in Pure Water and Combustion of Solid Fuels

John S. Corsi,[†,∥] Jintao Fu,[†] Zeyu Wang,[†,‡] Timothy Lee,[†] Alexander K. Ng,[†,§] and Eric Detsi*[,†,∥]

[†]Department of Materials Science & Engineering, University of Pennsylvania, Philadelphia, Pennsylvania 19104-6272, United States

[‡]State Key Laboratory of Advanced Welding and Joining, Harbin Institute of Technology, No.92, Xidazhi Ave., Harbin, Heilongjiang Province 150001, China

[§]St. John's University, 8000 Utopia Pkwy, Jamaica, New York 11439, United States

[∥]Vagelos Institute for Energy Science and Technology (VIEST), 231 S. 34th Street, Philadelphia, Pennsylvania 19104, United States

Supporting Information

ABSTRACT: There are still many scientific and engineering challenges that need to be addressed before a true sustainable hydrogen economy can be realized. Three of these challenges include sustainable hydrogen generation without CO_2 emissions, effective storage of this hydrogen for specific applications, and expanding the limited existing hydrogen infrastructure. Here we demonstrate (i) the fabrication of hierarchical bulk nanoporous aluminum with the coexistence of macroscopic and mesoscopic ligament/pore structures, with the mesoscopic ligaments in the range of 10−20 nm; (ii) the use of this aluminum to produce hydrogen on-site with a yield of ∼52−90% by hydrolysis with "pure" water, without incorporation of any catalyst or reaction promoter in the aluminum-water system; and (iii) the combustion of this aluminum in air under ambient conditions, which implies that this material could be attractive as a combustion fuel catalyst, e.g., to enhance the ignition and combustion of solid propellants. The inclusion of secondary aluminum or carbon-free primary aluminum in our process will make it possible to produce hydrogen with reduced carbon footprint for on-site and on-board applications using only nanoporous aluminum and water.

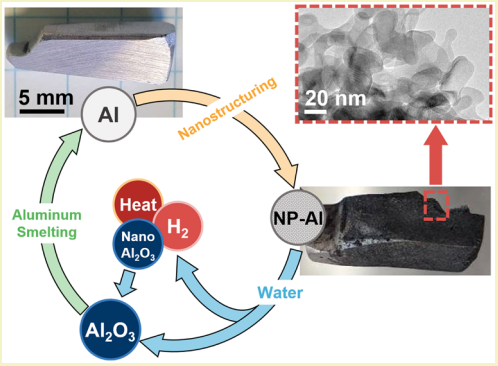

KEYWORDS: *Carbon-free hydrogen production, Fuel cell, Nanoporous aluminum, Pure water hydrolysis, Solid fuel combustion*

INTRODUCTION

Hydrogen, a highly abundant substance on Earth in the form of water, is a very promising energy carrier for producing electricity with zero-emissions upon reaction with oxygen for various applications including the transportation sector.[1−4] Of all common energy carrier media, hydrogen exhibits the highest gravimetric energy density of 142 MJ kg^{-1} compared to 47 MJ kg^{-1} for petroleum used in combustion engines.[1−3,5,6] Despite these remarkable features, there are still many scientific and engineering challenges that must be addressed before a true sustainable "hydrogen economy" can be realized. Three of these challenges include: (i) Sustainable hydrogen production: Over 95% of hydrogen used worldwide is produced through steam reforming of natural gas,[7−9] which is not a sustainable hydrogen production method because CO_2, a major greenhouse gas, is coproduced during steam reforming.[8] Alternatively, hydrogen can be produced in a sustainable manner by electrolysis of water.[10] However, the efficiency of this latter approach is fundamentally low,[11] since the electrical energy used to produce hydrogen is much higher than the energy that one can get back from this hydrogen. Therefore, scalable routes to generate hydrogen without any CO_2 footprint are still desirable. (ii) Hydrogen storage: Assuming hydrogen can be produced successfully in a sustainable manner, proper storage of this hydrogen prior to usage poses another major challenge.[12] This is because hydrogen is a low density gas at room temperature, which takes up a lot of space.[6,12] Solid-state hydrogen storage has been proposed, but materials for practical and reversible solid-state hydrogen storage are still under development.[13−16] The use of pressurized gas cylinders is the most promising approach used to store hydrogen for on-site and on-board applications.[17,18] However, the storage capacity of compressed hydrogen tanks is restricted due to safety considerations associated with high-pressure flammable gases.[19,20] (iii) Hydrogen infrastructure: While hydrogen fuel cell vehicles are increasing in popularity, their widespread adoption is in part impeded by the limited number of hydrogen refueling

Received: January 24, 2019
Revised: May 19, 2019
Published: May 24, 2019

DOI: 10.1021/acssuschemeng.9b00481
ACS Sustainable Chem. Eng. 2019, 7, 11194−11204

stations worldwide. For instance, there are currently less than 40 refueling stations in the US, much of which are concentrated in California. To overcome the three issues presented above in (i), (ii), and (iii), hydrogen generation by hydrolysis of water-reactive materials for on-board and on-site applications (i.e., without the need of storing this hydrogen) has been suggested.[4,21−24] For example, upon contact with water, reactive metals such as Al and Zn can produce hydrogen, heat, and the corresponding metal hydroxide through the following equations:[4,22]

$$2Al(s) + 6H_2O(l) \rightarrow 2Al(OH)_3(s) + 3H_2(g) + heat \quad (1)$$

$$Zn(s) + 2H_2O(l) \rightarrow Zn(OH)_2(s) + H_2(g) + heat \quad (2)$$

Even though the reactions in eqs 1 and 2 are thermodynamically favorable, they are self-limiting and do not continually proceed because the metal hydroxide layer (or "oxide" layer depending on the specific reaction conditions[4]) coproduced during the process forms an envelope around the metal surface at the beginning of the reaction. This hydroxide envelope prevents water from coming into direct contact with the metal underneath.[4] Several methods have been proposed to overcome the water-blocking hydroxide layer in order to allow the metal to fully react. These methods include:

(a) Disruption of the hydroxide envelope through incorporation of catalysts and reaction promoters such as salts, Ga, Li, In, and Sn in the metal to make aluminum-salts mixtures or alloys with a high water-reactivity.[4,25−29]
(b) Disruption of the hydroxide envelope through addition of catalysts and reaction promoters in water, such as NaCl, NaOH, and various metal oxides in the powder form.[4,23,24,30,31]

However, these methods have not resulted in a significant breakthrough in the field.[4] This is partly because the use of catalysts and reaction promoters significantly lowers the theoretical gravimetric hydrogen generation capacity of the metal-water system, since additional materials that are inactive toward hydrogen generation are considered "dead" mass. Additionally, in terms of recyclability, foreign substances (i.e., catalysts and reaction promoters) added to the metal-water system will be present as impurities in the aluminum hydroxide coproduced during hydrogen generation. These impurities are undesirable because they need to be removed through a complex purification process (i.e., Bayer process) prior to aluminum recovery from aluminum hydroxide.[32,33] For the present work, instead of modifying the chemical composition, we propose to modify the microstructure of the metal through nanoengineering. Indeed, the reactions in eqs 1 and 2 are self-limiting only in bulk materials. In other words, these reactions will fully proceed if the size of the metal is "small" enough. In this work, we hypothesize that the ideal size of the metal should be comparable to the thickness of the metal hydroxide envelope formed during the process, which in the case of aluminum hydroxide has been reported to be around ∼3.5 nm.[34] Based on our hypothesis, nanostructured aluminum with particles size around ∼7 nm (i.e., twice the thickness of the hydroxide envelope) should fully react with water to produce aluminum hydroxide and hydrogen gas with a yield of 100%. To verify our hypothesis, we introduce hierarchical nanoporosity in the bulk of aluminum. This hierarchical porosity is characterized by the coexistence of both macroscopic and mesoscopic ligament/pore structures. The mesoscopic ligaments in the range of 10−20 nm were found to actively react with water to produce hydrogen with a yield of ∼52−90%, without incorporation of any catalyst or reaction promoter in the aluminum-water system. In this hierarchical architecture, the macroscopic pores facilitate the flow of water through the bulk of aluminum, allowing the mesoscopic ligaments to react with water, as recently reported in our previous work on hydrolysis of hierarchical nanoporous Zn in distilled water.[22] Aluminum is the ideal candidate material for this application since it is the most abundant metal on Earth's crust. Furthermore, aluminum exhibits one of the highest hydrogen generation capacities at 3.7 wt % compared to 1.97 wt % for Zn. In subsequent sections, we demonstrate the feasibility of hydrogen generation for on-site applications using the hierarchical nanoporous aluminum-water system without the need to store this hydrogen. Here we focus on the following critical steps:

(1) Fabrication of oxide-free hierarchical bulk nanoporous Al with ultrafine ligaments in the range of 10−20 nm by electrolytic removal of sacrificial Mg from Al−Mg parent alloys with near-eutectic composition.
(2) Full recovery of the sacrificial Mg simultaneously during the electrolytic leaching process. Recovered Mg can be reused to make new Al−Mg parent alloys.
(3) Use of the fabricated hierarchical nanoporous Al with water to produce hydrogen, heat, and aluminum hydroxide, all of which are commercially relevant. Hydrogen gas is produced with a yield in the range of ∼52−90% through eq 1.
(4) In addition, the combustion of this bulk nanoporous aluminum in air and under ambient conditions is demonstrated, which makes this material attractive as a catalyst for solid fuel combustion.[35]

RESULTS AND DISCUSSION

Preparation of the Parent Alloy. Al−Mg parent alloy with near-eutectic composition was used for the fabrication of hierarchical nanoporous Al. In this section we present the characterization of this parent alloy, which was made by melting pure Al and pure Mg (see the Experimental Section). Two microstructural phases were present in the fabricated near-eutectic Al−Mg alloy,[36] as expected from the Al−Mg equilibrium phase diagram. These phases can be distinguished from the low-magnification scanning electron micrograph in Figure 1a, where the dark area corresponds to (Mg) solid solution,[36] and the light area represents β-$Al_{12}Mg_{17}$ intermetallic (the alloy surface was pretreated by etching to enhance the phase contrast).[36] Note that it is possible to identify these two phases from low-magnification imaging because the alloy surface was pretreated with acid (see the Experimental Section) to initiate the corrosion process; since the (Mg) phase dissolves faster than the β-$Al_{12}Mg_{17}$ intermetallic phase after surface treatment, the two phases can be dissociated from low-magnification electron micrographs. The fabricated parent alloy was further characterized by XRD to confirm the presence of these two phases. The green curve in Figure 1b represents the typical XRD pattern of the Al−Mg parent alloy. All the diffraction peaks from this pattern match the hexagonal Mg metal ($P6_3/mmc$) with PDF reference card number 00-004-0770 as depicted by the blue stick pattern in Figure 1b; and the cubic $Al_{12}Mg_{17}$ ($I\bar{4}3m$) with PDF reference card number 01-073-1148 as depicted by the

DOI: 10.1021/acssuschemeng.9b00481
ACS Sustainable Chem. Eng. 2019, 7, 11194−11204

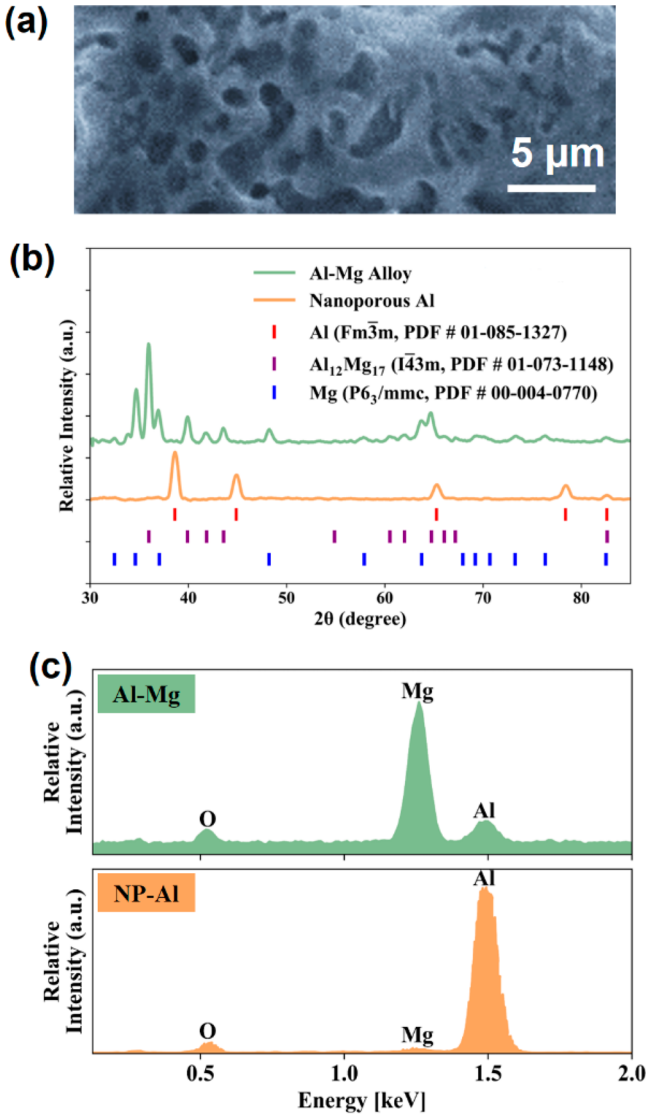

Figure 1. (a) SEM of the starting Al−Mg parent alloy with the surface pretreated to enhance the contrast between the (Mg) phase (dark) and β-$Al_{12}Mg_{17}$ phase (light). (b) XRD data for the Al−Mg parent alloy before (green) and after (orange) dealloying, together with crystallography data of Al (red), $Al_{12}Mg_{17}$ (purple), and Mg (blue). (c) EDS data of the Al−Mg parent alloy before (green) and after (orange) dealloying.

purple stick pattern in Figure 1b. Finally, the real chemical composition of the fabricated Al−Mg parent alloy with nominal composition $Al_{30}Mg_{70}$ at. % was investigated by EDS and ICP. The green EDS spectrum in Figure 1c shows the typical elemental composition of this alloy. Al and Mg signals are observed as expected. Quantitatively, EDS data suggest that the alloy composition is $Al_{24}Mg_{76}$ at. %, which corresponds to a hypoeutectic composition.[36] The small oxygen signal observed on the EDS spectrum of the parent alloy can be attributed to the native oxide formed upon reaction of Mg and Al with air. Because the interaction volume sampled by the electron beam is relatively shallow in EDS, the chemical composition obtained from EDS is more a representation of the near-surface composition. Therefore, ICP was used to determine the bulk composition of our alloy,[22] which was found to be ~$Al_{37}Mg_{63}$ at. % (i.e., hypereutectic composition[36]). Both EDS and ICP data are summarized in Table 1 below.

Table 1. ICP and EDS Elemental Composition Analysis of the Al−Mg Parent Alloy before and after Dealloying

		Al (at. %)	Mg (at. %)
before dealloying	ICP[a]	36.6	63.4
	EDS	24	76
after dealloying	ICP[a]	94.3	5.7
	EDS	98	2

[a]The samples before and after dealloying were dissolved in a mixture of HNO_3 and HCl for ICP analysis.

Hierarchical Nanoporous Aluminum. In this section, we demonstrate the fabrication of hierarchical nanoporous Al with ultrafine ligament/pore structures using a novel air-free electrolytic dealloying route in nonaqueous electrolytes.[37] Although a wide range of nanoporous metals[38−53] and nanoporous metalloids[54−57] have been fabricated using the conventional chemical and electrolytic dealloying route in "aqueous" electrolytes, these aqueous electrolytes are not suitable for the fabrication of reactive nanoporous metals,[22] such as nanoporous Al, because ionic species such as H^+ and OH^- present in aqueous electrolytes will spontaneously react with Al. In a first attempt to overcome this limitation, Detsi and Tolbert demonstrated the fabrication of ultrafine nanoporous Al with ligament size in the range of ~10 nm by galvanic replacement in nonaqueous electrolytes.[58] Detrimental side reactions occur during this galvanic replacement dealloying reaction, including the codeposition (plating) of Al concurrently during selective leaching of Mg, which result in severe structural coarsening (i.e., large ligaments). To avoid this coarsening issue, Detsi and Tolbert used a two-step synthesis route involving the formation of ultrafine nanoporous aluminum hydride composite structures by galvanic replacement, followed by heat-induced hydrogen desorption from these hydrides to obtain nanoporous Al with ligament size in the range of ~10 nm.[58] Recently, Jin and co-workers also exploited the galvanic replacement method to fabricate nanoporous Al with ligament size in the range of 200 nm.[59] In the present work, to overcome the limitation of the galvanic replacement approach (i.e., codeposition of Al and structural coarsening), we use a novel air-free nonaqueous electrolytic dealloying method.[37] In this approach, the reduced working ion in the nonaqueous electrolyte (i.e., Mg^{2+}) is the same nature as the sacrificial element (i.e., Mg) in the Al−Mg parent alloy. In such a configuration it is possible to electrochemically remove Mg from the starting Al−Mg alloy and plate it onto the counter electrode, resulting in the simultaneous recovery of the sacrificial element during selective leaching. Such a recovery of the sacrificial material is not possible during dealloying by galvanic replacement, or during conventional dealloying in aqueous electrolyte where the sacrificial element is not the same nature as the reduced working ion. In our work, the electrolytic cell configuration consists of a 3-neck round-bottom flask with the Al−Mg parent alloy used as the working electrode, a pure Mg foil used as the counter and reference electrodes, and 0.4 M all-phenyl complex (APC) electrolyte used as Mg-ion conducting electrolyte. The APC electrolyte was prepared following the procedure from our previous work.[60] The selective leaching process was carried out under inert atmosphere in an argon-filled MBraun glovebox with H_2O and O_2 content below 0.1 ppm.[60] All the experiments were performed at room temperature under ambient pressure in the glovebox. Note that the use of argon as inert gas in the

DOI: 10.1021/acssuschemeng.9b00481
ACS Sustainable Chem. Eng. 2019, 7, 11194−11204

glovebox is not critical; a nitrogen environment could be used as well. Furthermore, a glovebox itself is not the only equipment to carry out this electrolytic dealloying. Indeed, air-free electrolytic dealloying can be performed using an appropriate cell such as the one shown in supporting Figure S1, which was designed to perform this class of air-sensitive synthesis outside the glovebox. Mg was selectively removed from the Al−Mg parent alloy using electrolytic dealloying under potentiostatic control.[61,62] During potentiostatic controlled electrolytic dealloying, a constant voltage is maintained between the working and reference electrodes in order to dissolve Mg, and the corresponding Mg dissolution current between the working and counter electrodes is measured.[62] Figure 2a shows the typical electrolytic cell configuration before dealloying. A starting bulk piece of Al−Mg alloy with dimensions in the centimeter range was used as the working electrode and a Mg foil of similar size was used as both the counter and reference electrodes. Figure 2b shows the cell configuration after dealloying, as well as the fabricated bulk piece of nanoporous Al. The dealloyed nanoporous Al was broken into two pieces to demonstrate its brittleness, which is a common property of dealloyed nanoporous metals.[63] The Mg foil counter electrode after dealloying is also shown in Figure 2b. It can be seen that the surface of this Mg foil, which was initially smooth and dull before dealloying (see Figure 2a) has become very rough and shiny after dealloying. This is a result of the Mg plating process which occurs during selective leaching. To verify the chemical nature of the plated Mg, it was scraped from the counter electrode, collected in the powder form, and melted into a monolithic piece for characterization by XRD (see Figure 2c) and EDS. Both characterization methods confirm the formation of high purity Mg.

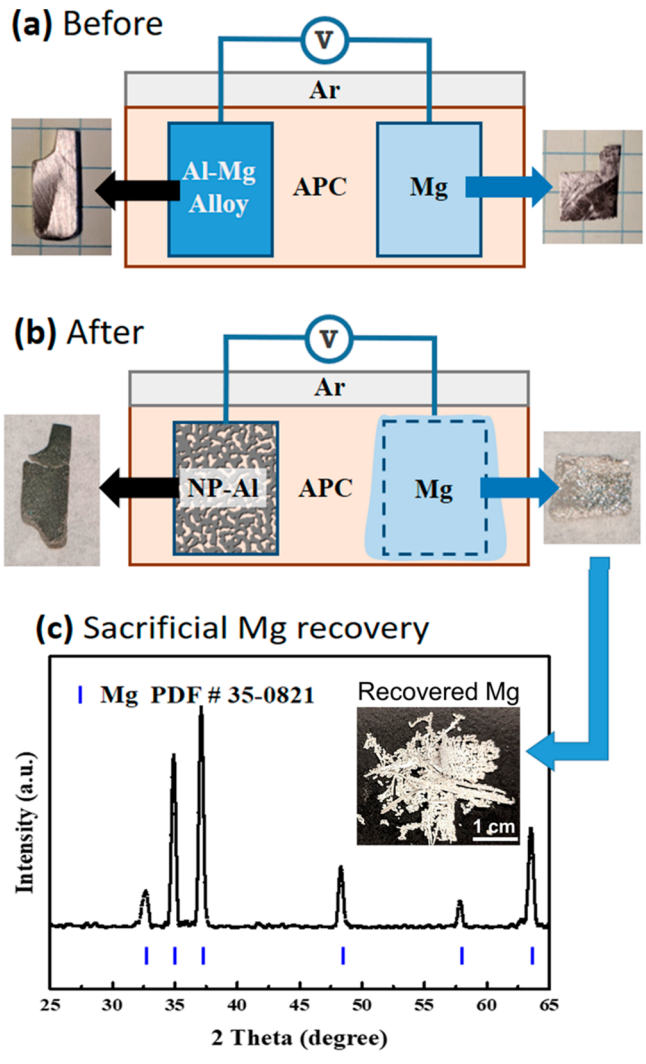

Figure 2. (a) Schematic of the electrolytic cell setup before dealloying. The cell contains an Al−Mg parent alloy used as the working electrode and Mg foil used as counter and reference electrodes in APC electrolyte. The cell operates is an argon environment. (b) Corresponding schematic of the electrolytic cell after dealloying. The starting Al−Mg working electrode is converted into nanoporous Al. Meanwhile Mg removed from this parent alloy is plated onto the Mg foil counter electrode. (c) XRD data of stripped Mg recovered on the counter electrode after dealloying.

The green line in Figure 3 represents a typical current profile as a function of time associated with Mg removal from the Al−Mg working electrode and Mg plating onto the Mg foil counter electrode at a constant potential of 450 mV versus Mg/Mg^{2+}. By integrating this current with respect to time, the total (cumulative) electric charge transferred during dealloying can be calculated. Faraday's laws of electrolysis were then used to convert this cumulative charge into the mass of Mg removed from the starting Al−Mg working electrode[61] and plated on the Mg counter electrode during dealloying as shown by the orange curve in Figure 3.[61] The electrolytic dealloying process was finished when the mass of Mg from the starting Al−Mg alloy was comparable to the mass of Mg calculated using the Faraday's laws of electrolysis.[61] The inset table in Figure 3 contains these gravimetric data for the working and counter electrodes before and after dealloying. It can be seen that the decrease in mass of the starting Al−Mg working electrode after dealloying is comparable to the increase in mass of the Mg foil counter electrode after dealloying. These gravimetric data further show that Mg removed from the working electrode can be efficiently collected on the counter electrode. This Mg could be reused to fabricate a new Al−Mg parent alloy, which makes this novel dealloying process sustainable. Note that while a thick (~4 mm) working electrode was used in Figure 3 to demonstrate how robust nanostructured bulk materials can be produced using this method, thinner electrodes can be used

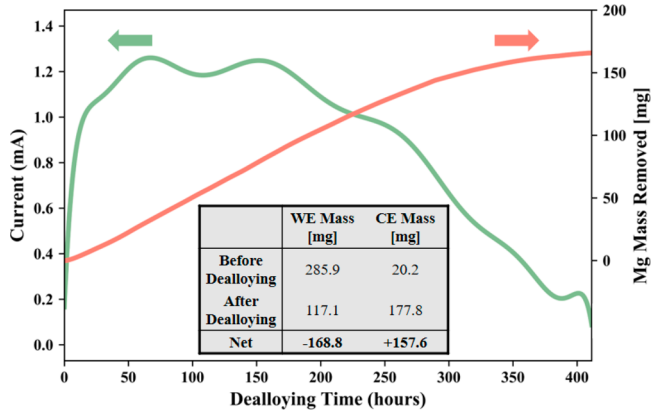

Figure 3. Cell current profile associated with electrolytic dealloying at a constant potential of 450 mV vs Mg/Mg^{2+} (green, left); and corresponding mass of Mg removed during dealloying (red, right). Summary of gravimetric electrode data (inset table).

DOI: 10.1021/acssuschemeng.9b00481
ACS Sustainable Chem. Eng. 2019, 7, 11194−11204

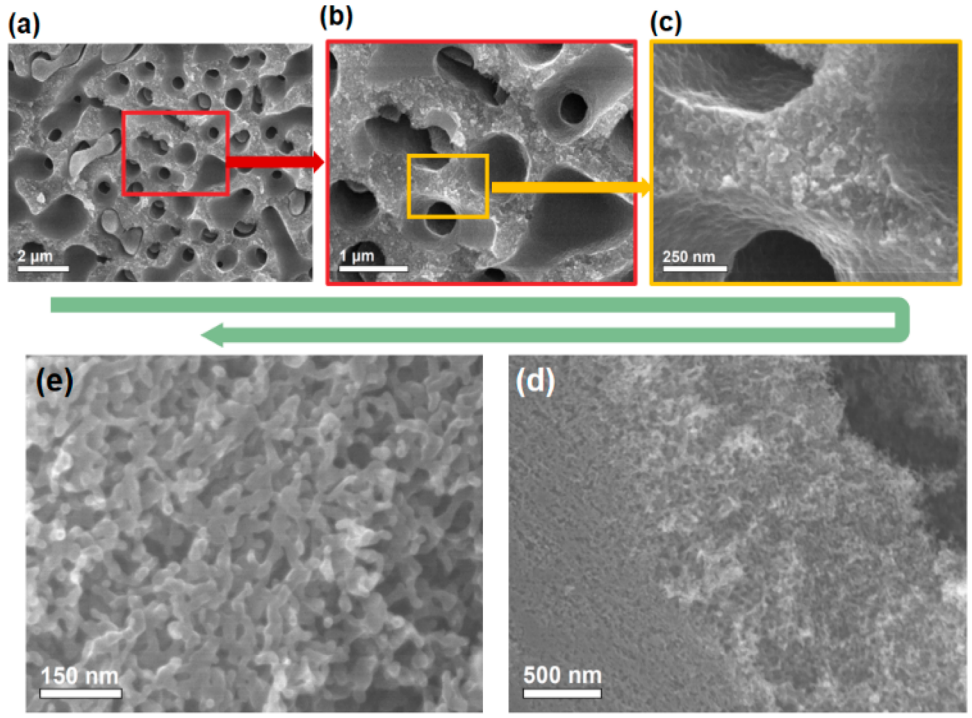

Figure 4. SEM of the fabricated hierarchical nanoporous Al at various magnifications. Large macropores and macroligaments with average feature size in the range of ~0.5−1 μm are observed at low magnifications (a,b). At intermediate magnifications (c) and at high magnifications (d,e) it is seen that the macroligaments are made of ultrafine mesoscopic ligament/pore structures.

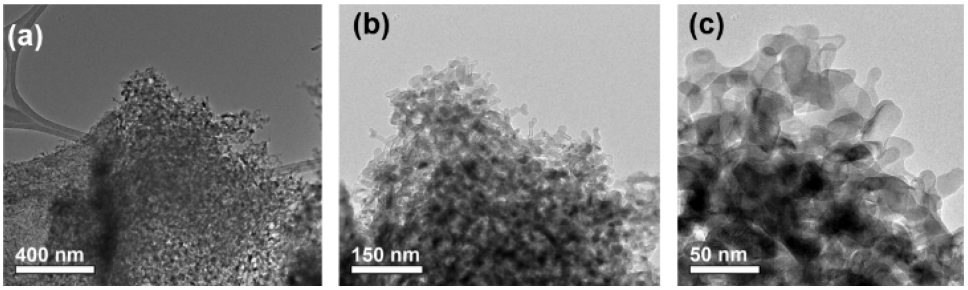

Figure 5. TEM of nanoporous Al at various magnifications. (a,b) At low and intermediate magnifications the material is composed of a dense network of ligaments. (c) At high magnification, the characteristic ligaments size is in the range of 10−20 nm.

to significantly decrease dealloying time. Typically, samples with thickness in the range of few micrometers can be dealloyed in about 45 h irrespective of the lateral dimensions of these samples as shown in Figure S2a. Indeed, it is important to realize that the lateral dimensions of the sample do not affect the dealloying time. Only the thickness is shown to have a critical impact on the dealloying time as illustrated in Figure S2b. In other words, for large-scale synthesis of nanoporous aluminum, at least one dimension of the sample should be in the range of a few micrometers. Therefore, we propose the use of Al−Mg parent materials in the powder form in combination with the setup schematized in Figure S 2d and S2e to scale up this synthesis. Dealloyed nanoporous Al was characterized by XRD, EDS, ICP, SEM, and TEM. The material was sealed in Kapton tape prior to XRD characterization in order to prevent it from reacting with air.[22] The orange pattern in Figure 1b represents the typical XRD pattern of the nanoporous Al after dealloying. All of the diffraction peaks in this pattern match with Al metal (PDF reference card number 01-085-1327) as depicted by the red stick pattern in Figure 1b. Also, the orange EDS spectrum in Figure 1c shows the typical elemental composition of the nanoporous Al after dealloying. It is seen that the dominant Mg peak in the Al−Mg parent alloy before dealloying (green EDS spectrum Figure 1c) almost entirely vanishes after dealloying (orange EDS spectrum Figure 1c). The content of residual Mg in nanoporous Al after dealloying was found to be 2 at. % from EDS data and 5.7 at. % from ICP data. Detailed EDS and ICP data are summarized in Table 1.

Scanning and transmission electron micrographs of the dealloyed nanoporous Al are displayed at different magnifications in Figures 4 and 5, respectively. Large macropores and macroligaments with average feature size in the range of ~0.5−1 μm are observed from SEM images at low magnifications as depicted in Figure 4a,b. The large macropores come from the full dissolution of the (Mg) solid solution phase from the Al−Mg parent alloy. According to the Al−Mg equilibrium phase diagram, the maximum solubility of Al in the (Mg) phase near room temperatures is less than 2 at. %. Consequently, such a small amount of Al is etched away together with the (Mg) matrix, resulting in the large macropores and macroligaments. At intermediate (Figure 4c) magnifications and high

DOI: 10.1021/acssuschemeng.9b00481
ACS Sustainable Chem. Eng. 2019, 7, 11194−11204

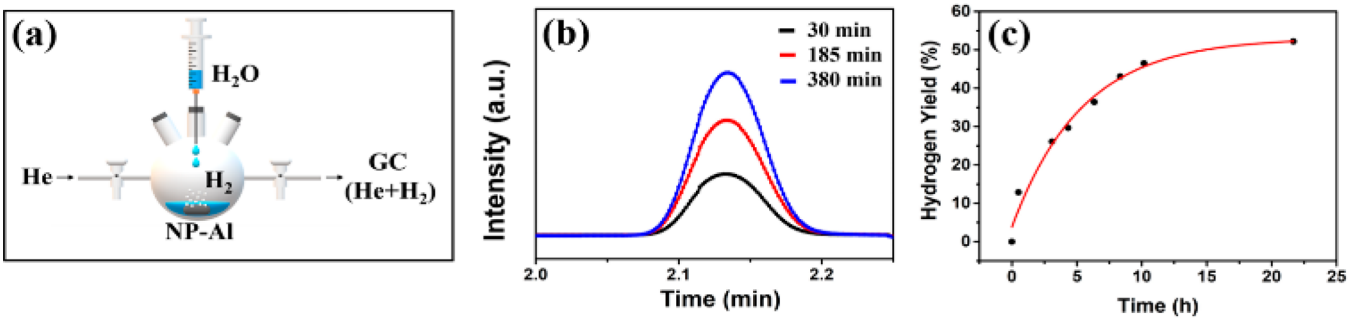

Figure 6. (a) Schematic of the setup for hydrogen measurement during GC experiments. (b) Typical raw GC data associated with the amount of hydrogen produced 30, 185, and 380 min after injection of water, respectively. (c) Cumulative amount of hydrogen produced after 22 h.

magnifications (Figure 4d,e), it can be seen that the macroligaments are composed of ultrafine mesoscopic ligament/pore structures. These mesoscopic structures were characterized using TEM as seen in Figure 5b,c; the average ligament size was found to be in the range 10−20 nm. The small nanoscale pores come from the selective dissolution of Mg from the β-$Al_{12}Mg_{17}$ phase.

Hydrogen Generation by Hydrolysis of Hierarchical Nanoporous Al in "Pure" Water. *In Situ Gas Chromatography Study of Hydrogen Generation by Hydrolysis of Hierarchical Nanoporous Al in Pure Water.* In this section, the amount and rate of hydrogen generated through the reaction of the fabricated hierarchical bulk nanoporous Al with deionized water (eq 1) is quantitatively investigated using a customized Scion 456 gas chromatography (GC) system.[22] The schematic setup for hydrogen measurement is shown in Figure 6a. In order to prevent rapid oxidation in air, the piece of bulk nanoporous Al used for hydrogen generation was brought in the reaction flask inside an argon-filled glovebox, and the flask was sealed before taking it outside the glovebox for GC measurements. Deionized water was then injected into the reaction flask using a syringe (see Figure 6a).

Note that deionized water is used to emphasize that our hierarchical nanoporous Al-water system can produce hydrogen without any additives in water. Helium was used as a carrier gas to transfer hydrogen produced from the reaction flask to the GC. The black, red and blue curves in Figure 6b show typical raw GC data associated with the amount of hydrogen produced 30, 185, and 380 min after injection of water, respectively. As time increases, the cumulative amount of hydrogen generated also increases. A similar trend was previously observed during hydrolysis of hierarchical nanoporous Zn in distilled water.[22] Figure 6c shows the cumulative amount of hydrogen produced as a function of total reaction time. In the first 30 min, hydrogen generation rate was found to be ∼0.5 mg/min per gram of nanoporous Al, which corresponds to ∼5.3 mL/min per gram of Al. The average hydrogen generation rate after 10 h was about ∼1 mL/min per gram of Al. For the sake of comparison, the average hydrogen generation rate from hierarchical bulk nanoporous Zn was reported to be ∼7.3 μg/min per gram of Zn, corresponding to 0.08 mL/min per gram of Zn.[22] Therefore, it can be concluded that in the first 30 min, hydrogen generation rate by hydrolysis of hierarchical nanoporous Al is more than 66 times faster than generating hydrogen by hydrolysis of hierarchical nanoporous Zn.[22] After a significant drop in the hydrogen generation rate of the Al-water system after ∼22 h, the hydrogen generation yield deduced from the total amount of hydrogen gas collected was found to be ∼52% of the theoretical gravimetric capacity of this Al-water system (i.e., ∼1.92 wt % compared to 3.7 wt %). For comparison, a yield of 20% of the theoretical gravimetric capacity of the Zn-water system was achieved during hydrogen generation by hydrolysis of hierarchical nanoporous Zn in distilled water (i.e., 0.39 wt % compared to 1.97 wt %).[22] This remarkable performance (i.e., faster rate, higher capacity) of hierarchical nanoporous Al can be attributed to the nearly oxide-free nature of the surface of fabricated nanoporous Al (i.e., absence of Al_2O_3), as it will be clarified in the next section using XPS analysis. In contrast, the surface of nanoporous Zn was covered with oxygen species because it was fabricated in air using "aqueous" corroding medium Zn.[22]

Next, the reaction rate of our bulk nanoporous aluminum with water to produce hydrogen was further compared with the reaction rate of other reported Al-based materials systems in literature. However, this is not a fair comparison because we do not include any additives in the aluminum-water system unlike other reported works, which use additives to enhance the reactivity of aluminum with water.[27,64,65] Producing hydrogen from aluminum and water without any additives presents several advantages for practical applications as mentioned earlier. Data on hydrogen generation rate are shown in Table 2. Even though no additives are used in the present work, in general our reaction rate is competitive.

Ex Situ X-ray Photoelectron Spectroscopy of Study of Hydrolyzed Nanoporous Al. The hydrogen generation yield of ∼52% reported above from GC data is an underestimated value because the hydrolysis process was stopped after 22 h

Table 2. Literature Data on Hydrogen Generation Rate in Al-Based Systems with and without Additives (Nanoporous Zn Is Included Because It Was Also Discussed in This Manuscript)

material	additive	rate [g H_2/s/g material]	ref
bulk nanoporous aluminum	none	8.33×10^{-6}	this work
ball milled and quenched activated aluminum	none	8×10^{-7}	4
aluminum	γ-Al_2O_3	4×10^{-6}	4
aluminum at 55 °C	KCl, NaCl	2×10^{-4}	4
aluminum	$Al(OH)_3$	3.4×10^{-4}	23
aluminum	0.10 M Na_2SnO_3	no mass given	24
aluminum	Ga−In, gallam (70:30, 7 wt %)	1.9×10^{-3}	25
bulk nanoporous Zn	none	1.2×10^{-7}	22

DOI: 10.1021/acssuschemeng.9b00481
ACS Sustainable Chem. Eng. 2019, 7, 11194−11204

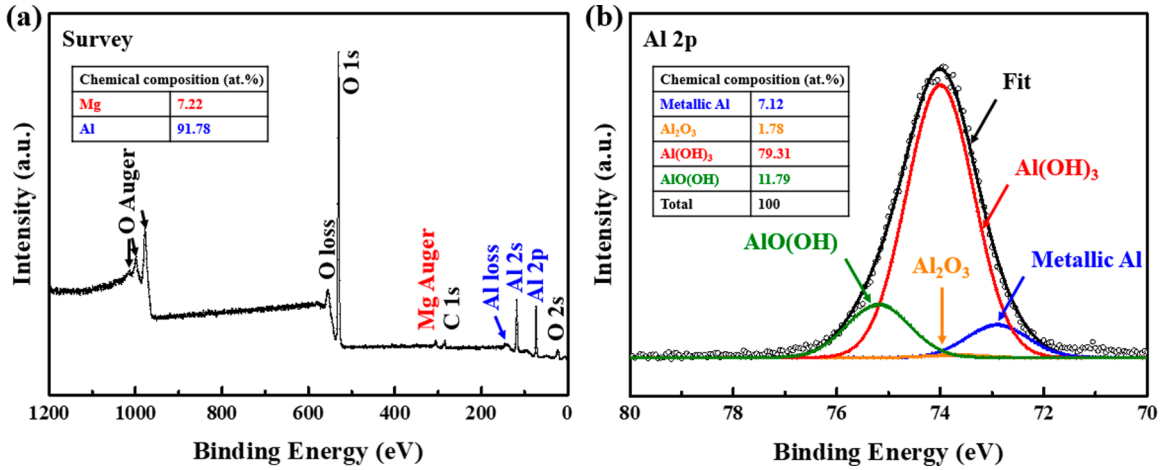

Figure 7. (a) XPS survey spectrum of the $Al(OH)_3$ solid byproduct formed during the reaction of hierarchical nanoporous Al with water. (b) XPS high resolution core level spectrum of the Al 2p. The corresponding chemical composition given in the inset table.

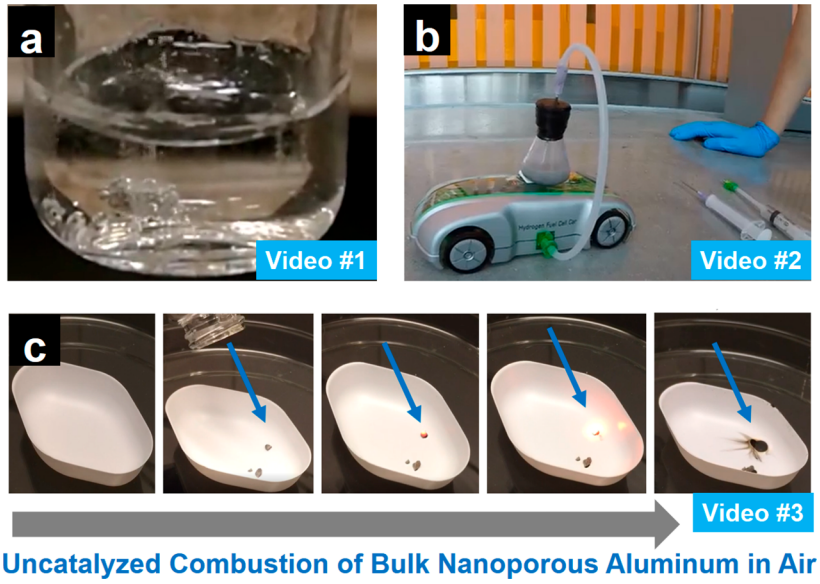

Figure 8. (a) Hydrogen generation from the reaction of our bulk nanoporous Al with pure water. (b) Toy fuel cell vehicle powered by hydrogen from the reaction of nanoporous Al and water. (c) Combustion of bulk nanoporous Al in air. See the Supporting Information, Videos 1−3, for these processes.

due to a significant drop in hydrogen generation rate. The sample was kept one more day in water to ensure completion of the reaction. XPS characterization was then performed to investigate the oxidation state of Al in the solid $Al(OH)_3$ byproduct formed through the reaction of hierarchical nanoporous Al with water. Note that due to the relatively small penetration depth in XPS, the sample was crushed into powder prior to XPS characterization in order to expose the inert parts of the material during XPS. The XPS survey spectrum reveals obvious O and Al peaks, as shown in Figure 7a. In addition to O and Al, a small amount of Mg (amount: 7.2 at. % compared to 91.8 at. % of Al) was detected, suggesting the presence of a tiny fraction of residual Mg in the dealloyed nanoporous Al, in agreement with EDS and ICP data as discussed previously in Table 1. Figure 7b displays a high-resolution Al 2p core level spectrum. As expected, the deconvolution of this Al 2p reveals the predominance of Al−OH peak at ∼74 eV from the $Al(OH)_3$ compound.[66] In addition to $Al(OH)_3$, three other Al states were identified: metallic Al peak at ∼72.9 eV, Al−O peak at ∼73.7 eV from Al_2O_3, and finally O═Al−OH peak at ∼75.2 eV from the AlO(OH) compound.[66,67] The atomic fractions of all these compounds are shown in the inset table of Figure 7b. The fraction of Al in the form $Al(OH)_3$ was found to be 79.31 at. %, suggesting that the reaction yield during hydrolysis of Al to make hydrogen gas and $Al(OH)_3$ through eq 1 is at least 79.31%. It can be seen that 7.12 at. % of metallic Al is present, indicating that our hierarchical nanoporous Al has not fully reacted with water to produce hydrogen. The presence of unreacted aluminum can be rationalized by the 10−20 nm mesoscopic ligament size distribution in this hierarchical nanoporous Al. Based on our hypothesis stated earlier, the ideal size of Al for its full reaction with water is on the order of ∼7 nm. In the 10−20 nm ligament size distribution, ligaments near the lower limit (i.e., 10 nm) are susceptible to fully react with water, while ligaments near the upper limit (i.e., 20 nm) will only partially react with water. Therefore, the partially reacted ligaments account for the presence of metallic Al in the

DOI: 10.1021/acssuschemeng.9b00481
ACS Sustainable Chem. Eng. 2019, 7, 11194−11204

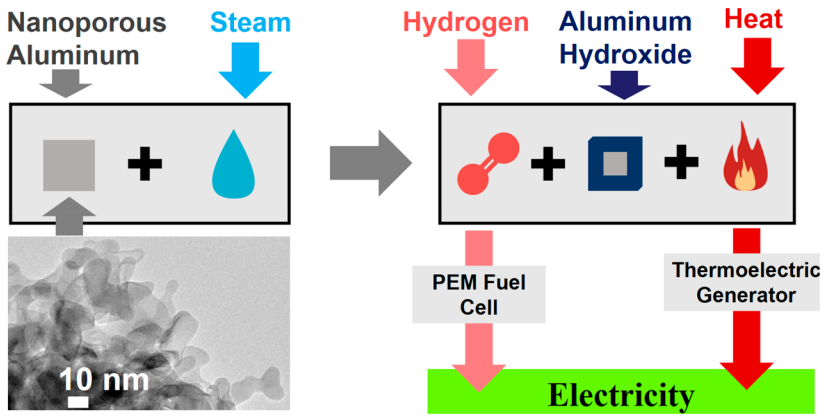

Figure 9. Hydrogen and heat generated from the reaction of bulk nanoporous Al with steam is used to produce electricity.[37]

solid byproduct. Furthermore, a 11.79% fraction of AlO(OH) was detected and can be attributed to the gradual conversion of $Al(OH)_3$ into AlO(OH) when this material dehydrates during vacuum exposure and X-ray irradiation needed in XPS characterization. It should be emphasized that only traces of Al_2O_3 were found (1.78 at. %), suggesting that the nanoporous Al had not been exposed to oxygen during the fabrication process. The maximum hydrogen generation yield was deduced from the total fraction of $Al(OH)_3$ and AlO(OH) compounds, assuming that AlO(OH) evolves from $Al(OH)_3$. This gives a total yield of 91.10%.

On-Board Hydrogen Generation and Combustion of Bulk Nanoporous Aluminum in Air. This section is aimed at demonstrating the feasibility of on-board hydrogen generation by hydrolysis of hierarchical nanoporous Al in deionized water without incorporation of any catalysts or reaction promoters in the Al-water system. In addition, the combustion of bulk nanoporous aluminum in air is also demonstrated. At first, for the reader to visualize and appreciate the process of hydrogen generation by hydrolysis of bulk nanoporous aluminum in pure water, a video was made to illustrate this phenomenon (see also Figure 8a). This video is available in the Supporting Information as Video 1. Next, a hierarchical bulk nanoporous Al sample was crushed into powder to further enhance its hydrogen generation kinetics when in contact with water. This powder was used to produce hydrogen on-board and feed a fuel cell toy vehicle (Horizon's H-racer 2.0 Educational Kit, http://www.horizoneducational.com/juniorproducts/h-racer/), which normally operates with hydrogen generated off-board by water electrolysis (see Figure 8b). The corresponding video is available in the Supporting Information as Video 2.

Finally, while catalysts and high temperatures are usually needed to ignite solid materials in the bulk form, our bulk nanoporous aluminum can be ignited in air (i.e., with oxygen is the oxidant) at room temperature without the use of any catalysts as shown in Figure 8c and in the Supporting Information, Video 3. This implies that bulk nanoporous aluminum itself can be used as a combustion catalyst, e.g. in solid fuel rocket propulsion applications.[35]

Energy is stored in aluminum when thermal and electrical energies are used to convert aluminum oxide feedstock into metallic aluminum during aluminum smelting. This energy is released from nanoporous aluminum in the form of heat during its combustion in air. Another way to recover this energy is through the exothermic reaction that we used in eq 1 to produce hydrogen by hydrolysis of aluminum with water (see also Figure 9). The amount of energy stored in 1 kg of energy of hydrogen is approximately 142 MJ.[68] Interestingly, about 142 MJ of heat is also generated when 1 kg of hydrogen is produced through the reaction of aluminum and water as depicted in Figure 9.[68] Both heat and hydrogen can be converted into electricity using a fuel cell (for hydrogen) and a thermoelectric generator (for the heat) as illustrated in Figure 9.[37]

Sustainability and Cost. Hydrogen produced from nanoporous aluminum and water can only be considered sustainable if there is no greenhouse gas emissions during the process, including processing of primary dense aluminum used to make our nanoporous aluminum. There are many energy intensive processes involved in primary aluminum extraction including: Removal of impurity from its bauxite ore to obtain pure $Al(OH)_3$, conversion of this $Al(OH)_3$ to Al_2O_3 at high temperatures and electrolysis of Al_2O_3 in molten cryolite at temperatures above 1000 °C to make metallic aluminum and oxygen gas through eq 3.[32,33,69]

$$2Al_2O_3(l) \rightarrow 4Al(l) + 3O_2(g) \quad (3)$$

Fortunately, thermal energy stored in aluminum during smelting can be recovered in our process during the combustion or hydrolysis of nanoporous aluminum, as discussed in the previous section. However, because of the high temperature (>1000 °C) needed for the electrolysis step during aluminum smelting, the carbon-based anodes used in the electrolysis cell react with O_2 (generated through eq 3) to produce CO_2. Therefore, the current pathway to extract aluminum is not sustainable because of the high carbon footprint. One way to produce sustainable hydrogen from our nanoporous aluminum could be through the use of recycled secondary aluminum (i.e., scrap aluminum). The 2016 global annual market of high purity secondary aluminum was over 22 million tons, meaning that there is enough secondary aluminum to integrate in our process for large scale production of hydrogen with reduced carbon footprint. Besides secondary aluminum, recent news suggest that carbon-free aluminum is expected to be commercialized in the near future by Elysis (https://elysis.com/en), a joint venture composed of high profile aluminum suppliers (Rio Tinto and Alcoa), and aluminum consumers (such as Apple). Elysis has developed an efficient, carbon-free aluminum smelting process through the use of alternative materials to carbon electrodes, to serve as the high temperature electrode for traditional aluminum smelting. The inclusion of this carbon-free aluminum in our

DOI: 10.1021/acssuschemeng.9b00481
ACS Sustainable Chem. Eng. 2019, 7, 11194−11204

process would allow for sustainable hydrogen to be produced from primary aluminum. In terms of the cost, for hydrogen produced through our process to be affordable, the high purity aluminum hydroxide coproduced during hydrolysis of nanoporous aluminum can be further heat-treated to make nanostructured alumina with high specific surface area, also known as activated alumina. Activated alumina is highly valuable and can be sold to reduce the cost of hydrogen. Indeed, activated alumina is used in several applications including: Fluoride adsorbents for water treatment, catalysts and catalyst−supports, desiccants, bioceramics, and separators for lithium-ion battery. The 2016 global annual market of activated alumina was over 11 million tons, suggesting that activated alumina produced from our process during large scale hydrogen generation is unlikely to saturate the global activated alumina market. In a follow-up work, we have shown that aluminum hydroxide coproduced with hydrogen during hydrolysis of nanoporous aluminum in pure water can be converted into activated alumina with specific surface area over 190 m^2/g. This follow-up work will be published elsewhere.

CONCLUSION

In this work, we demonstrate the synthesis of hierarchical bulk nanoporous Al through a unique nonaqueous electrolytic dealloying process that also allows for the simultaneous recovery of the sacrificial material (metallic Mg) selectively stripped from the parent alloy (Al−Mg alloy). The fabricated hierarchical nanoporous aluminum is made of macroscopic and mesoscopic ligament/pore structures with average characteristic sizes in the range of 10−20 nm for the mesoscopic ligaments. XPS data reveal that the nanoporous Al was not exposed to oxygen during its processing. This material was used to produce hydrogen on-site with a yield in the range of ∼52−90% by hydrolysis with deionized water, and without using any additives in the aluminum-water system to promote the reaction. The spontaneous combustion of bulk nanoporous aluminum in air and at ambient conditions was also demonstrated in this work. Such materials are desirable as catalysts in solid combustion fuels. In terms of hydrogen generation by hydrolysis in water, a major advantage of the hierarchical porosity is that the large pores can facilitate the transfer of water through the bulk of aluminum, allowing the mesoscopic ligaments to come in direct contact with water and react to produce hydrogen and heat. The large pores also facilitate the transfer of hydrogen gas out of the bulk of the material. This approach could be attractive for large-scale sustainable hydrogen production using only water and aluminum through the utilization of secondary aluminum or potentially carbon-free primary aluminum which is currently being developed by Elysis (https://elysis.com/en).

EXPERIMENTAL SECTION

Al−Mg parent alloys with near-eutectic composition were made by homogeneously melting pure Al and pure Mg at 750 °C in a graphite crucible using a quartz tube under argon flow in combination with a tube furnace (OTF-1200X, MTI Corporation).[70] The nominal composition was taken to be $Al_{30}Mg_{70}$ at. %. Nanoporous Al was fabricated by selective electrolytic removal of Mg from the above-mentioned Al−Mg parent alloys using a Bio-Logic VMP-300 multichannel potentiostat/galvanostat.[60] A JEOL 7500F scanning electron microscope (SEM) equipped with energy dispersive X-ray spectroscopy (EDS) capability was used to characterize the microstructure and elemental composition of the fabricated Al−Mg parent alloy and corresponding dealloyed nanoporous Al. Inductively coupled plasma optical emission spectroscopy (Spectro Genesis ICP-OES device) was also used to further investigate the bulk chemical compositions of these materials. The X-ray diffraction (XRD) data of these materials was taken with a Rigaku D/Max-B X-ray diffractometer with Bragg − Brentano parafocusing geometry operating with Cu Kα1 line (λ = 1.5405 Å) and a horizontal goniometer collecting at an angle range of 10−95° with 0.05° step size and 2°/min scanning speed, with a conventional copper target X-ray tube set to 40 kV and 30 mA. A customized gas chromatograph system (GC, Scion 456) equipped with pulsed discharge detector (PDD) with 5 Å molecular sieve packed column, and thermal conductivity detector (TCD) was used to measure the amount and rate of hydrogen produced during the reaction of nanoporous aluminum with water.[22] X-ray photoelectron spectroscopy (XPS) was carried out utilizing a PHI Veraprobe 5000 instrument equipped with a monochromated Al Kα radiation source in order to investigate the chemical composition of the solid product formed during the reaction of Al with water.

ASSOCIATED CONTENT

Supporting Information

The Supporting Information is available free of charge on the ACS Publications website at DOI: 10.1021/acssuschemeng.9b00481.

Process of hydrogen generation by hydrolysis of bulk nanoporous aluminum in pure water (AVI)

Powder used to produce hydrogen on-board and feed a fuel cell toy vehicle (AVI)

Bulk nanoporous aluminum that can be ignited in air (i.e., with oxygen is the oxidant) at room temperature without the use of any catalysts (AVI)

Important factors involved in scaling up this synthesis process including: a glassware for containing sealed inert environment outside of glovebox, the effect of decreased electrode thickness on dealloying current, and comments on electrode dimensions and design (PDF)

AUTHOR INFORMATION

Corresponding Author

*E-mail: detsi@seas.upenn.edu.

ORCID

Eric Detsi: 0000-0002-4009-7260

Notes

The authors declare no competing financial interest.

ACKNOWLEDGMENTS

The authors are thankful to Penn Engineering and NSF for the financial supports through the PI startup and the NSF-EAGER program with Award number: CMMI-1840672. The authors are also thankful to the Vagelos Institute for Energy Science and Technology (VIEST) for the support through the VIEST Graduate Fellowship support. Lastly, the authors would like to acknowledge the Singh Center for Nanotechnology, part of the National Nanotechnology Coordinated Infrastructure Program, which is supported by the National Science Foundation grant NNCI-1542153.

REFERENCES

(1) Mazloomi, K.; Gomes, C. Hydrogen as an Energy Carrier: Prospects and Challenges. *Renewable Sustainable Energy Rev.* **2012**, *16*, 3024−3033.

(2) Züttel, A.; Remhof, A.; Borgschulte, A.; Friedrichs, O. Hydrogen: The Future Energy Carrier. *Philos. Trans. R. Soc., A* **2010**, *368*, 3329−3342.

(3) Dinga, G. P. Hydrogen: The Ultimate Fuel and Energy Carrier. *Int. J. Hydrogen Energy* **1989**, *14*, 777−784.
(4) Petrovic, J.; Thomas, G. Reaction of Aluminum with Water to Produce Hydrogen. *US Dep. Energy* **2008**, 1−26.
(5) Midilli, A.; Ay, M.; Dincer, I.; Rosen, M. A. On Hydrogen and Hydrogen Energy Strategies I : Current Status and Needs. *Renewable Sustainable Energy Rev.* **2005**, *9*, 255−271.
(6) Durbin, D. J.; Malardier-Jugroot, C. Review of Hydrogen Storage Techniques for on Board Vehicle Applications. *Int. J. Hydrogen Energy* **2013**, *38*, 14595−14617.
(7) Nikolaidis, P.; Poullikkas, A. A Comparative Overview of Hydrogen Production Processes. *Renewable Sustainable Energy Rev.* **2017**, *67*, 597−611.
(8) Kothari, R.; Buddhi, D.; Sawhney, R. L. Comparison of Environmental and Economic Aspects of Various Hydrogen Production Methods. *Renewable Sustainable Energy Rev.* **2008**, *12*, 553−563.
(9) Bartels, J. R.; Pate, M. B.; Olson, N. K. An Economic Survey of Hydrogen Production from Conventional and Alternative Energy Sources. *Int. J. Hydrogen Energy* **2010**, *35*, 8371−8384.
(10) Zeng, K.; Zhang, D. Recent Progress in Alkaline Water Electrolysis for Hydrogen Production and Applications. *Prog. Energy Combust. Sci.* **2010**, *36*, 307−326.
(11) Elam, C. C.; Padró, C. E. G.; Sandrock, G.; Luzzi, A.; Lindblad, P.; Hagen, E. F. Realizing the Hydrogen Future: The International Energy Agency's Efforts to Advance Hydrogen Energy Technologies. *Int. J. Hydrogen Energy* **2003**, *28*, 601−607.
(12) David, W. I. F. Effective Hydrogen Storage: A Strategic Chemistry Challenge. *Faraday Discuss.* **2011**, *151*, 399−414.
(13) Lim, K. L.; Kazemian, H.; Yaakob, Z.; Daud, W. R. W. Solid-State Materials and Methods for Hydrogen Storage: A Critical Review. *Chem. Eng. Technol.* **2010**, *33*, 213−226.
(14) Rusman, N. A. A.; Dahari, M. A Review on the Current Progress of Metal Hydrides Material for Solid-State Hydrogen Storage Applications. *Int. J. Hydrogen Energy* **2016**, *41*, 12108−12126.
(15) Krishnan, G.; De Graaf, S.; Ten Brink, G. H.; Verheijen, M. A.; Kooi, B. J.; Palasantzas, G. Shape and Structural Motifs Control of MgTi Bimetallic Nanoparticles Using Hydrogen and Methane as Trace Impurities. *Nanoscale* **2018**, *10*, 1297−1307.
(16) Krishnan, G.; De Graaf, S.; Ten Brink, G. H.; Persson, P. O. Å.; Kooi, B. J.; Palasantzas, G. Strategies to Initiate and Control the Nucleation Behavior of Bimetallic Nanoparticles. *Nanoscale* **2017**, *9*, 8149−8156.
(17) Jorgensen, S. W. Hydrogen Storage Tanks for Vehicles: Recent Progress and Current Status. *Curr. Opin. Solid State Mater. Sci.* **2011**, *15*, 39−43.
(18) De Miguel, N.; Ortiz Cebolla, R.; Acosta, B.; Moretto, P.; Harskamp, F.; Bonato, C. Compressed Hydrogen Tanks for On-Board Application: Thermal Behaviour during Cycling. *Int. J. Hydrogen Energy* **2015**, *40*, 6449−6458.
(19) Utgikar, V. P.; Thiesen, T. Safety of Compressed Hydrogen Fuel Tanks: Leakage from Stationary Vehicles. *Technol. Soc.* **2005**, *27*, 315−320.
(20) Hua, T. Q.; Ahluwalia, R. K.; Peng, J.-K.; Kromer, M.; Lasher, S.; McKenney, K.; Law, K.; Sinha, J. Technical Assessment of Compressed Hydrogen Storage Tank Systems for Automotive Applications. *Int. J. Hydrogen Energy* **2011**, *36*, 3037−3049.
(21) Erogbogbo, F.; Lin, T.; Tucciarone, P. M.; Lajoie, K. M.; Lai, L.; Patki, G. D.; Prasad, P. N.; Swihart, M. T. On-Demand Hydrogen Generation Using Nanosilicon: Splitting Water without Light, Heat, or Electricity. *Nano Lett.* **2013**, *13*, 451−456.
(22) Fu, J.; Deng, Z.; Lee, T.; Corsi, J. S.; Wang, Z.; Zhang, D.; Detsi, E. PH-Controlled Dealloying Route to Hierarchical Bulk Nanoporous Zn Derived from Metastable Alloy for Hydrogen Generation by Hydrolysis of Zn in Neutral Water. *ACS Appl. Energy Mater.* **2018**, *1*, 3198−3205.
(23) Chen, Y. K.; Teng, H.; Te; Lee, T. Y.; Wang, H. W. Rapid Hydrogen Generation from Aluminum-Water System by Adjusting Water Ratio to Various Aluminum/Aluminum Hydroxide. *Int. J. Energy Environ. Eng.* **2014**, *5*, 1−6.
(24) Soler, L.; Candela, A. M.; Macanás, J.; Muñoz, M.; Casado, J. Hydrogen Generation from Water and Aluminum Promoted by Sodium Stannate. *Int. J. Hydrogen Energy* **2010**, *35*, 1038−1048.
(25) Ilyukhina, A. V.; Ilyukhin, A. S.; Shkolnikov, E. I. Hydrogen Generation from Water by Means of Activated Aluminum. *Int. J. Hydrogen Energy* **2012**, *37*, 16382−16387.
(26) Rosenband, V.; Gany, A. Application of Activated Aluminum Powder for Generation of Hydrogen from Water. *Int. J. Hydrogen Energy* **2010**, *35*, 10898−10904.
(27) Wang, H. Z.; Leung, D. Y. C.; Leung, M. K. H.; Ni, M. A Review on Hydrogen Production Using Aluminum and Aluminum Alloys. *Renewable Sustainable Energy Rev.* **2009**, *13*, 845−853.
(28) Huang, X. N.; Lv, C. J.; Huang, Y. X.; Liu, S.; Wang, C.; Chen, D. Effects of Amalgam on Hydrogen Generation by Hydrolysis of Aluminum with Water. *Int. J. Hydrogen Energy* **2011**, *36*, 15119−15124.
(29) Zhao, Z.; Chen, X.; Hao, M. Hydrogen Generation by Splitting Water with Al-Ca Alloy. *Energy* **2011**, *36*, 2782−2787.
(30) Soler, L.; Candela, A. M.; Macanás, J.; Muñoz, M.; Casado, J. In Situ Generation of Hydrogen from Water by Aluminum Corrosion in Solutions of Sodium Aluminate. *J. Power Sources* **2009**, *192*, 21−26.
(31) Ma, G. L.; Dai, H. B.; Zhuang, D. W.; Xia, H. J.; Wang, P. Controlled Hydrogen Generation by Reaction of Aluminum/Sodium Hydroxide/Sodium Stannate Solid Mixture with Water. *Int. J. Hydrogen Energy* **2012**, *37*, 5811−5816.
(32) Habashi, F. A Hundred Years of the Bayer Process for Alumina Production. *Essential Readings in Light Metals* **2016**, *1*, 85−93.
(33) Misra, C. Aluminum Oxide (Alumina), Hydrated. *Kirk-Othmer Encycl. Chem. Technol.* **2003**, *2*, 421−433.
(34) Phambu, N. Characterization of Aluminum Hydroxide Thin Film on Metallic Aluminum Powder. *Mater. Lett.* **2003**, *57*, 2907−2913.
(35) Maggi, F.; Dossi, S.; Paravan, C.; DeLuca, L. T.; Liljedahl, M. Activated Aluminum Powders for Space Propulsion. *Powder Technol.* **2015**, *270*, 46−52.
(36) Zhang, Z. M.; Lii, T.; Xu, C. J.; Guo, X. F. Microstructure of Binary Mg-Al Eutectic Alloy Wires Produced by the Ohno Continuous Casting Process. *Acta Metall. Sin. (Engl. Lett.)* **2008**, *21*, 275−281.
(37) Detsi, E.; Corsi, J. S. Bulk Nanoporous Materials For On-Board Generation Of Hydrogen And Other Products. U.S. Provisional Appl. No. US62/644,972, 2018 2018.
(38) Erlebacher, J.; Aziz, M. J.; Karma, A.; Dimitrov, N.; Sieradzki, K. Evolution of Nanoporosity in Dealloying. *Nature* **2001**, *410*, 450−453.
(39) Detsi, E.; Vuković, Z.; Punzhin, S.; Bronsveld, P. M.; Onck, P. R.; Hosson, J. T. M. D. Fine-Tuning the Feature Size of Nanoporous Silver. *CrystEngComm* **2012**, *14*, 5402−5406.
(40) Weissmüller, J.; Sieradzki, K. Dealloyed Nanoporous Materials with Interface-Controlled Behavior. *MRS Bull.* **2018**, *43*, 14−19.
(41) Lilleodden, E. T.; Voorhees, P. W. On the Topological, Morphological, and Microstructural Characterization of Nanoporous Metals. *MRS Bull.* **2018**, *43*, 20−26.
(42) Chen, Q.; Ding, Y.; Chen, M. Nanoporous Metal by Dealloying for Electrochemical Energy Conversion and Storage. *MRS Bull.* **2018**, *43*, 43−48.
(43) Cortie, M. B.; Maaroof, A. I.; Smith, G. B. Electrochemical Capacitance of Mesoporous Gold. *Gold Bull.* **2005**, *38*, 14−22.
(44) Tai, M. C.; Gentle, A.; Arnold, M. D.; Cortie, M. B. Optical in Situ Study of De-Alloying Kinetics in Nanoporous Gold Sponges. *RSC Adv.* **2016**, *6*, 85773−85778.
(45) Zhang, Z.; Wang, Y.; Qi, Z.; Zhang, W.; Qin, J.; Frenzel, J. Generalized Fabrication of Nanoporous Metals (Au, Pd, Pt, Ag, and Cu) through Chemical Dealloying. *J. Phys. Chem. C* **2009**, *113*, 12629−12636.

DOI: 10.1021/acssuschemeng.9b00481
ACS Sustainable Chem. Eng. 2019, 7, 11194−11204

(46) Hayes, J. R.; Hodge, A. M.; Biener, J.; Hamza, A. V.; Sieradzki, K. Monolithic Nanoporous Copper by Dealloying Mn−Cu. *J. Mater. Res.* **2006**, *21*, 2611−2616.
(47) Cook, J. B.; Detsi, E.; Liu, Y.; Liang, Y.-L.; Kim, H.-S.; Petrissans, X.; Dunn, B.; Tolbert, S. H. Nanoporous Tin with a Granular Hierarchical Ligament Morphology as a Highly Stable Li-Ion Battery Anode. *ACS Appl. Mater. Interfaces* **2017**, *9*, 293−303.
(48) Meng, F.; Ding, Y. Sub-Micrometer-Thick All-Solid-State Supercapacitors with High Power and Energy Densities. *Adv. Mater.* **2011**, *23*, 4098−4102.
(49) Lang, X.; Hirata, A.; Fujita, T.; Chen, M. Nanoporous Metal/Oxide Hybrid Electrodes for Electrochemical Supercapacitors. *Nat. Nanotechnol.* **2011**, *6*, 232−236.
(50) Hakamada, M.; Mabuchi, M. Fabrication of Nanoporous Palladium by Dealloying and Its Thermal Coarsening. *J. Alloys Compd.* **2009**, *479*, 326−329.
(51) Dorofeeva, T. S.; Seker, E. Electrically Tunable Pore Morphology in Nanoporous Gold Thin Films. *Nano Res.* **2015**, *8*, 2188−2198.
(52) Detsi, E.; Punzhin, S.; Rao, J.; Onck, P. R.; De Hosson, J. T. M. Enhanced Strain in Functional Nanoporous Gold with a Dual Microscopic Length Scale Structure. *ACS Nano* **2012**, *6*, 3734−3744.
(53) Wittstock, A.; Zielasek, V.; Biener, J.; Friend, C. M.; Bäumer, M. Nanoporous Gold Catalysts for Selective Gas-Phase Oxidative Coupling of Methanol at Low Temperature. *Science (Washington, DC, U. S.)* **2010**, *327*, 319−322.
(54) Liu, S.; Feng, J.; Bian, X.; Liu, J.; Xu, H. The Morphology-Controlled Synthesis of a Nanoporous-Antimony Anode for High-Performance Sodium-Ion Batteries. *Energy Environ. Sci.* **2016**, *9*, 1229−1236.
(55) Maxwell, T. L.; Balk, T. J. The Fabrication and Characterization of Bimodal Nanoporous Si with Retained Mg through Dealloying. *Adv. Eng. Mater.* **2018**, *20*, 1700519.
(56) Liu, S.; Feng, J.; Bian, X.; Qian, Y.; Liu, J.; Xu, H. Nanoporous Germanium as High-Capacity Lithium-Ion Battery Anode. *Nano Energy* **2015**, *13*, 651−657.
(57) Ma, W.; Wang, J.; Gao, H.; Niu, J.; Luo, F.; Peng, Z.; Zhang, Z. A Mesoporous Antimony-Based Nanocomposite for Advanced Sodium Ion Batteries. *Energy Storage Mater.* **2018**, *13*, 247−256.
(58) Tolbert, S. H.; Detsi, E. Hydrogen Storage in Nanoporous and Nanostructured Hydride Forming Metals, 2013, US20180016139A1, U.S. Patent.
(59) Yang, W.; Zheng, X.; Wang, S.; Jin, H. *J. Electrochem. Soc.* **2018**, *165*, 492−496.
(60) Yaghoobnejad Asl, H.; Fu, J.; Kumar, H.; Welborn, S. S.; Shenoy, V. B.; Detsi, E. In Situ Dealloying of Bulk Mg 2 Sn in Mg-Ion Half Cell as an Effective Route to Nanostructured Sn for High Performance Mg-Ion Battery Anodes. *Chem. Mater.* **2018**, *30*, 1815−1824.
(61) Detsi, E.; Van De Schootbrugge, M.; Punzhin, S.; Onck, P. R.; De Hosson, J. T. M. On Tuning the Morphology of Nanoporous Gold. *Scr. Mater.* **2011**, *64*, 319−322.
(62) Ma, K.; Corsi, J. S.; Fu, J.; Detsi, E. Origin of the Volume Contraction during Nanoporous Gold Formation by Dealloying for High-Performance Electrochemical Applications. *ACS Appl. Nano Mater.* **2018**, *1*, 541−546.
(63) Detsi, E.; Sellès, M. S.; Onck, P. R.; De Hosson, J. T. M. Nanoporous Silver as Electrochemical Actuator. *Scr. Mater.* **2013**, *69*, 195−198.
(64) Alinejad, B.; Mahmoodi, K. A Novel Method for Generating Hydrogen by Hydrolysis of Highly Activated Aluminum Nanoparticles in Pure Water. *Int. J. Hydrogen Energy* **2009**, *34*, 7934−7938.
(65) Mahmoodi, K.; Alinejad, B. Enhancement of Hydrogen Generation Rate in Reaction of Aluminum with Water. *Int. J. Hydrogen Energy* **2010**, *35*, 5227−5232.
(66) Seo, Y. I.; Lee, Y. J.; Kim, D.-G.; Lee, K. H.; Kim, Y. Do. Mechanism of Aluminum Hydroxide Layer Formation by Surface Modification of Aluminum. *Appl. Surf. Sci.* **2010**, *256*, 4434−4437.
(67) Andreeva, R.; Stoyanova, E.; Tsanev, A.; Stoychev, D. Influence of the Surface Pre-Treatment of Aluminum on the Processes of Formation of Cerium Oxides Protective Films. In Journal of Physics: Conference Series; 2016.
(68) Shkolnikov, E. I.; Zhuk, A. Z.; Vlaskin, M. S. Aluminum as Energy Carrier: Feasibility Analysis and Current Technologies Overview. *Renewable Sustainable Energy Rev.* **2011**, *15*, 4611−4623.
(69) Tabereaux, A. T.; Peterson, R. D. Aluminum Production. *Treatise on Process Metallurgy* **2014**, *3*, 839−917.
(70) Detsi, E.; Petrissans, X.; Yan, Y.; Cook, J. B.; Deng, Z.; Liang, Y.-L.; Dunn, B.; Tolbert, S. H. Tuning Ligament Shape in Dealloyed Nanoporous Tin and the Impact of Nanoscale Morphology on Its Applications in Na-Ion Alloy Battery Anodes. *Phys. Rev. Mater.* **2018**, *2*, 055404.

DOI: 10.1021/acssuschemeng.9b00481
ACS Sustainable Chem. Eng. 2019, 7, 11194−11204